PCCP

RSC Publishing

PAPER

Determination of two-photon photoactivation rates of fluorescent proteins

Cite this: *Phys. Chem. Chem. Phys.*, 2013, **15**, 14868

Tobias M. P. Hartwich,[abc] Fedor V. Subach,[d] Lynn Cooley,[e] Vladislav V. Verkhusha[d] and Joerg Bewersdorf*[afg]

Received 8th March 2013,
Accepted 4th July 2013

DOI: 10.1039/c3cp51035b

www.rsc.org/pccp

The application of two-photon activation of photoactivatable fluorescent proteins is limited by a lack of information about two-photon activation rates. Here we present rates for the commonly used photoactivatable proteins PAmCherry, PAmKate and PA-GFP at different wavelengths using a novel method that allows us to determine the two-photon activation rates directly, independent of any reference data, with microscopic sample volumes. We show that PAmCherry features the highest rates of the tested proteins at 700 nm activation wavelength followed by PAmKate. Towards longer wavelengths, two-photon activation rates decrease for all three proteins. For PAmCherry, our data contradicts an activation model relying solely on two-photon activation and suggests additional activation pathways requiring at least two absorption steps. Our method is readily expandable to other photoactivatable fluorescent molecules. The presented results allow optimization of experimental conditions in spectroscopic and imaging techniques such as super-resolution fluorescence microscopy.

Introduction

The advent of photoactivatable fluorescent proteins (PAFPs) has initiated a plethora of new imaging techniques. These proteins which change their emission characteristics upon irradiation with light, can be subdivided into four groups according to their switching process: irreversibly photoactivatable from a dark to a fluorescent state (such as PA-GFP[1] and PAmCherry1, further in this paper referred to as PAmCherry[2]), irreversibly photoconvertable from a green to a red fluorescent state (such as Kaede[3]), reversibly photoswitchable from a dark to a fluorescent state (such as rsTagRFP,[4] rsEGFP[5] and Dreiklang[6]) and both reversibly and irreversibly photoconvertable from a green to a red fluorescent state (such as IrisFP[7]).[8] Labeling target proteins with PAFPs instead of conventional FPs allows singling out protein sub-populations through light and has enabled researchers to probe cells and organisms in completely new ways. By activating only one cell, for example, individual cells can be followed over time.[9] Similarly, single organelles or even individual protein populations can be tracked to observe, for example, fusion dynamics or protein turnover.[9] Stochastic or targeted photoactivation/photoconversion/photoswitching of PAFPs allows to overcome the diffraction limit in microscopy achieving down to $\sim$10 nm spatial resolution.[10] PAFPs can even be used to fabricate optical storage devices.[5]

Most of these methods rely on PAFP-activation in a specific area of a sample while excluding the rest. The available spatial control is, however, limited since the (usually violet) light required for activation penetrates the whole sample and photoactivation is therefore not confined in depth. This leads to unwanted activation of PAFPs in out-of-focus planes and thereby to problematic background as well as photobleaching of these molecules. Analogous to two-photon excitation (2PE) microscopy,[11] this lack of spatial control can be resolved by utilizing two-photon (2P) absorption to confine photoactivation three-dimensionally: using near-infrared light where each photon carries only half of the necessary activation energy requires simultaneous absorption of two photons and thereby limits activation to the focus of a high-intensity laser beam. By scanning this laser focus, three-dimensional activation patterns can be created.

The possibility of using two-photon activation (2PA) for PAFPs and other photoactivatable probes has previously

[a] *Department of Cell Biology, Yale School of Medicine, New Haven, CT 06520, USA*
[b] *Department of Biophysical Chemistry, University of Heidelberg, 69120 Heidelberg, Germany*
[c] *Department of New Materials and Biosystems, Max Planck Institute for Metals Research, 70569 Stuttgart, Germany*
[d] *Department of Anatomy and Structural Biology and Gruss-Lipper Biophotonics Center, Albert Einstein College of Medicine, Bronx, NY 10461, USA*
[e] *Department of Genetics, Yale School of Medicine, New Haven, CT 06520, USA*
[f] *Department of Biomedical Engineering, Yale University, New Haven, CT 06511, USA*
[g] *Kavli Institute for Neuroscience, Yale University, New Haven, CT 06520, USA. E-mail: joerg.bewersdorf@yale.edu*

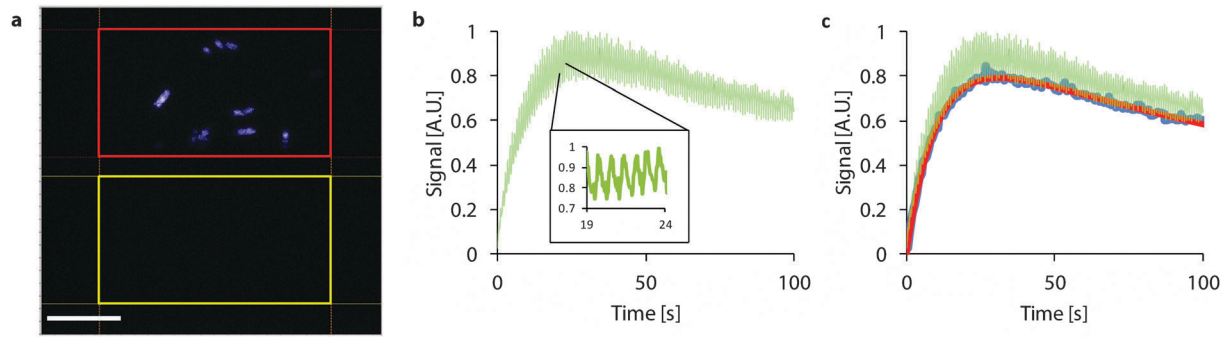

Fig. 1 Example of activation data acquisition. (a) Typical camera frame during acquisition. The fluorescence signal from the sample is imaged onto the upper region of the camera chip (red box) while the lower region (yellow box) only detects background signal. Scale bar: 10 μm. (b) Background-corrected signal over time. Inset highlights periodic modulation stemming from the axial scanning of the sample. (c) For further analysis only the lower boundary curve (blue) is used. Fitting a model function (red curve) to the boundary curve allows to extract rate parameters.

been demonstrated,[12–16] but only one study about Kaede has reported quantitative information about 2PA rates.[17] Here, we report the wavelength and power dependence of 2PA rates for a number of widely used PAFPs directly measured by a novel method which requires no knowledge of probe concentrations or diffusion coefficients. Our approach is readily applicable to all photoactivatable probes and requires only microscopic sample volumes under typical biological sample preparation conditions.

Methods

Bacterial cell culture

LMG194 bacteria carrying pBAD/HisB-PAFP plasmid were grown over night in LB medium supplemented with 100 μg ml^{-1} ampicillin and 0.004% arabinose. They were then washed twice in phosphate-based saline (PBS), fixed for 30 minutes in 4% paraformaldehyde at room temperature, and washed again three times in PBS. For imaging, 10–20 μl of the bacteria–PBS stock were added onto a poly-L-lysine coated cover slip, mounted on a microscope slide and sealed using two-component silicon glue.

Optical setup

All measurements were taken with a custom-built fluorescence microscope as described elsewhere.[18] In short, continuous-wave lasers (488 nm, 556 nm, 568 nm) were coupled into a standard inverted microscope stand for wide-field excitation. Additionally, a mode-locked Ti:sapphire laser (Mai Tai, Spectra-Physics, 80 MHz, <100 fs at the laser output) was focused into the sample and the diffraction-limited focus was scanned across the field of view (15×30 μm^2) in a Lissajous pattern for photoactivation. Fluorescence images were recorded with an electron-multiplying CCD camera.

Data recording and pre-processing

For each measurement, between 5000–50 000 frames were recorded at frame rates of 20–35 frames per second. Axial scanning, using a piezo actuator, is performed continuously over a range of 3 μm which exceeds the thickness of the sample. The sample is scanned in 10 steps with a step size of 300 nm pausing for 75 ms between steps.

The sample is either continuously exposed to activation and excitation light or illuminated alternatingly. Generated fluorescence from the sample is imaged onto a region of interest (ROI) of the camera while a second ROI detects only background signal (see Fig. 1a). For each frame, the signal in both ROIs is summed up and the value from the background ROI is subtracted from the other one to correct for background and camera offset. The resulting data (further called activation curve) shows a periodic modulation which is correlated to the performed axial scanning of the sample (see Fig. 1b). The periodic increase in signal is caused by 2P excited fluorescence of the activated species which increases the signal when the scanned laser beam is in the same plane as the imaged bacteria. The minima in the signal represent fluorescence excited by only the 488 nm, 556 nm or 568 nm laser. For further analysis, only the lower boundary curve (blue line in Fig. 1c) created from these minima is used which eliminates potential 2PE contributions.

Activation rate determination

To determine the 2PA rate we record activation curves at different activation intensities and wavelengths to characterize the nonlinear absorption process and to determine its spectral dependence. To resemble typical microscopy experiments, we use *E. coli* bacteria expressing PAFP in the cytoplasm and mounted in PBS between a standard cover slip and a microscope slide. Due to the high sensitivity of this method only microscopic sample quantities (~ 5 bacteria) are required per measurement.

In order to extract the activation rate from this activation curve we describe our system using a three-state model in which molecules turn from an initial non-activated state I into a fluorescent state F with an activation rate k_{act}. From there they transfer into a bleached state B described by a bleaching rate k_{bl}. This model is represented by the rate equations

$$\frac{dN_I(t)}{dt} = -k_{act}N_I(t) \quad (1)$$

$$\frac{dN_F(t)}{dt} = k_{act}N_I(t) - k_{bl}N_F(t) \quad (2)$$

$$\frac{dN_B(t)}{dt} = k_{bl} N_F(t) \quad (3)$$

where N_I, N_F and N_B represent the number of molecules in the respective states at each time point t. Solving this system of linear differential equations yields the number of fluorescent molecules as a function of time:

$$N_F(t) = A(e^{-k_{bl}(t-t_0)} - e^{-k_{act}(t-t_0)}) \quad (4)$$

Here A is an amplitude factor representing the total number of molecules in the observed sample volume and t_0 accounts for the possibility of molecules being already activated at the beginning of the measurement. Since the observed fluorescence signal is proportional to N_F, we fit the measured data using a function based on eqn (4) with the addition of a constant to account for background. Since no significant fraction of pre-activated PAFPs could be observed, we set t_0 to zero. The validity of this approach was confirmed by comparing fit results with and without setting t_0 to zero (data not shown).

Results and discussion

Activation rates

Fig. 2 shows the determined activation rates, k_{act}, for the widely used proteins PAmCherry (Fig. 2a), PAmKate[19] (Fig. 2b) and PA-GFP (Fig. 2c) as a function of the average activation laser power, P_{avg}, in the sample for different wavelengths. In our hands, the also examined PAFPs Dendra2[20] and mEos2[21] did not show sufficient activation using the Ti:sapphire laser to be quantifiable.

Measurements were repeated 3–14 times for different FOVs and samples at each wavelength and P_{avg}. For PAmKate and PA-GFP activation rates at very low activation powers were below our detection limit. Activation rates were observed to decrease with increasing wavelength. Fits of the data points with third-order polynomials show clear 2P dependence which is replaced by a third or higher order dependence for higher P_{avg}. PAmCherry was the only PAFP from the pool of our investigated proteins that exhibited significant activation by the readout laser.

A typical recorded activation curve using only the excitation laser at 556 nm and no activation laser can be seen in Fig. 3a (black curve). It exhibits a slow continuous increase due to the low activation rate associated to the 556 nm laser. Also shown is an activation curve using a 568 nm laser for excitation instead of the 556 nm laser (grey curve). This small shift in excitation wavelength suppresses any observable cross-talk activation and only reveals a slow decrease of the signal due to bleaching of background.

Observation of multistep activation processes during PAmCherry photoactivation

Despite the apparent lack of activation of PAmCherry by the 568 nm laser alone, we see a clear dependence of the activation rate on the 568 nm laser intensity when reverting to the original illumination scheme with both the excitation and the activation laser switched on (Fig. 3b). Higher 568 nm laser intensities

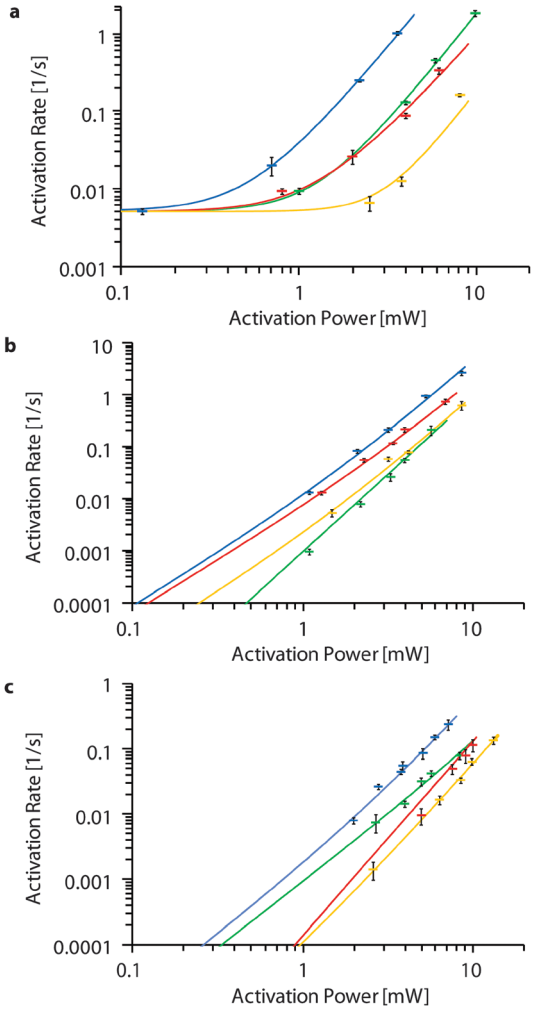

Fig. 2 Activation rates for PAmCherry (a), PAmKate (b) and PA-GFP (c) for different wavelengths (700 nm: blue, 800 nm: green, 900 nm: red, 1000 nm: yellow) as a function of activation power in the sample (PAmCherry: 556 nm excitation laser at 3.9 W cm^{-2}; PAmKate: 556 nm excitation laser at 3.6 W cm^{-2}; PA-GFP: 488 nm excitation laser at 22.2 mW cm^{-2}).

yield higher activation rates as is evident from the increasingly steeper slopes seen in Fig. 3b recorded at 7.3 W cm^{-2}, 14.7 W cm^{-2} and 34.0 W cm^{-2} of excitation intensity at 568 nm (2.0 mW activation laser power in the sample at 700 nm were used for all measurements). This indicates a previously unobserved complexity in the photoactivation process of PAmCherry.

To further probe this phenomenon, we altered our illumination style to a pattern in which we turn on the excitation and activation lasers in an interleaved fashion for the same durations of time. Fig. 4 shows a typical activation curve recorded with this new illumination pattern. The sample is alternatingly illuminated by the excitation laser at 568 nm (0.6 s, 4.7 W cm^{-2}) and the Ti:sapphire activation laser at 700 nm (0.6 s, 2.0 mW). Since PAmCherry can be activated but not efficiently excited at 700 nm, the signal drops to background level during the activation periods.

As can be seen in the close-up (inset Fig. 4), the signal shows no activation during the first excitation period of 0.6 s which

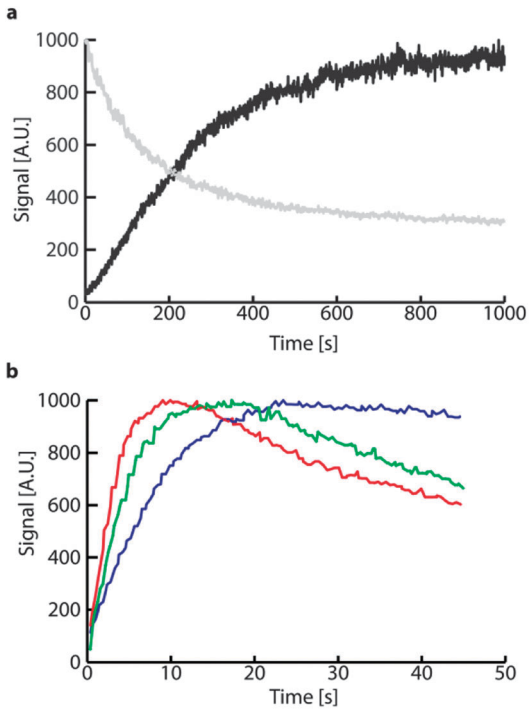

Fig. 3 Dependence on the excitation laser. (a) Recorded fluorescence signal for PAmCherry illuminated with 556 nm laser light at 3.6 W cm^{-2} (black curve) showing a slow increase in signal due to activation by the 556 nm laser, and by 568 nm laser light at 60.2 W cm^{-2} (grey curve) showing no activation and only a slow bleaching of the autofluorescent background. (b) Activation curves for PAmCherry recorded at 2.0 mW of 700 nm laser illumination and 7.3 W cm^{-2}, 14.7 W cm^{-2} and 34.0 W cm^{-2} of 568 nm laser illumination for the blue, green and red curve, respectively. The steepening of the activation slope with increasing 568 nm laser intensity demonstrates a dependence of the activation on the 568 nm laser. Please note, that all curves are normalized. The observed peak signals in (b) are about three orders of magnitude larger than the ones in (a).

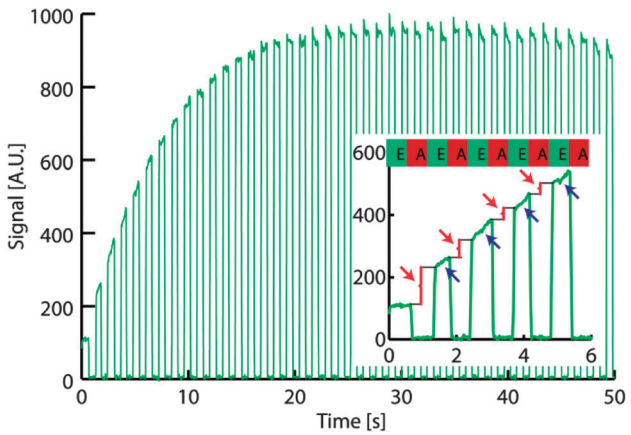

Fig. 4 Sequential illumination signal response. Recorded fluorescence signal using a sequential illumination scheme. Inset contains a close-up of first 6 seconds. The sequential illumination pattern is shown with excitation periods (green, 'E') and activation periods (red, 'A') at the top of the inset. Red arrows highlight step-like increases of fluorescence signal after activation periods. Blue arrows mark activation during excitation periods.

starts the experiment. This is in agreement with our previous result that the 568 nm laser alone is not sufficient to activate

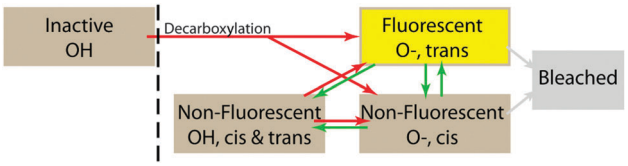

Scheme 1 Model of light-driven transitions during the activation of PAmCherry. The activation laser (near UV or two-photon illumination at ~700 nm; shown as red arrows) can pump molecules from the carboxylated and protonated state into the decarboxylated and deprotonated *cis* or *trans* state. Within decarboxylated states, the activation laser can trigger deprotonation whereas the excitation laser (568 nm; shown as green arrows) can switch molecules between their *cis* and *trans* forms and trigger protonation.

PAmCherry. The clear jumps in signal that happen during the activation periods (highlighted by the red arrows) are due to activation by the Ti:sapphire laser. Interestingly, however, the signals during the subsequent excitation periods which are each preceded by a 2PA period, show an increase in the amplitude as highlighted by the blue arrows. This cannot be explained by a simple one-step activation process.

An explanation for these observations lies in a more complex photoactivation mechanism of PAmCherry, which involves activated decarboxylated states described previously.[22] Our data is consistent with the following model: near-ultraviolet light or 2P absorption in the 700 nm range is required to initially decarboxylate the molecule. Several additional transitions are possible between decarboxylated states. Light at the excitation wavelength of 568 nm can switch the molecule between the *cis* and the *trans* states of (i) the deprotonated or (ii) protonated forms as well as (iii) from the deprotonated to the protonated form. Activation with near-ultraviolet light or by 2P absorption in the 700 nm range is, however, required to (iv) switch the molecule from a protonated back to a deprotonated form. Only the decarboxylated, deprotonated *trans* form is fluorescent. A schematic of these transitions is shown in Scheme 1 and explains all observed phenomena: in the interleaved activation scheme, following this model, a fraction of the PAmCherry molecules transitions out of the inactive state during the 2PA period and ends up in the non-fluorescent deprotonated *cis* form. During the excitation period some of these non-fluorescent molecules will then be pumped into the fluorescent state by light at 568 nm wavelength. This explains the observed increase in signal during the excitation period and the dependence of the activation rate on the intensity of the 568 nm excitation laser (in the interleaved as well as in the simultaneous illumination case).

Conclusions

We have reported 2PA rates for PAmCherry, PAmKate and PA-GFP, over a wavelength range ranging from 700 to 1000 nm for typical imaging conditions. Our data provides for the first time quantitative information about this important photophysical property for three of the most popular PAFPs. All tested PAFPs achieve highest activation rates at the lowest

wavelength used (700 nm). It is unclear whether lower wavelengths would result in even higher activation rates. 700 nm represents, however, a practical lower limit for most 2PA experiments because of the tuning range of available Ti:sapphire lasers as well as potential overlap with the emission spectra of red fluorophores. At a reasonable 2PA laser power in the sample of 1 mW and 700 nm wavelength and for low excitation intensities, PAmCherry activates about 3-fold faster than PAmKate and about 22-fold faster than PA-GFP. Based on the additional experiments with PAmCherry presented here, it can, however, be assumed that this ratio is likely to change for higher excitation intensities. Furthermore, our experiments have revealed a previously unobserved phenomenon of additional light-driven transitions for PAmCherry, which cannot be explained by a simple three-state model but are consistent with a mechanistic model reported previously.[22]

The presented results demonstrate the versatility of the reported method. We want to point out that our approach is not limited to PAFPs but can be readily expanded to other photoactivatable probes used in biomedical imaging (*e.g.* super-resolution microscopy) or microfabrication. Microscopic volumes are sufficient and applications are not limited to bacteria. In fact, any sample suitable for microscopy, such as cultured mammalian cells, tissue sections or single molecules on a cover slip, can be used.

Acknowledgements

We thank Prof. Joachim Spatz for support and Dr. Yang Yang, Dr. Neeraj Tiwari and Dr. Intaek Lee for helpful discussions. This work was supported by the grants GM091791 (to L.C. & J.B.) and GM073913 and CA164468 (to V.V.V.) from National Institutes of Health. J.B. declares significant financial interest in Vutara, Inc.

References

1 G. H. Patterson and J. Lippincott-Schwartz, *Science*, 2002, **297**, 1873–1877.
2 F. V. Subach, G. H. Patterson, S. Manley, J. M. Gillette, J. Lippincott-Schwartz and V. V. Verkhusha, *Nat. Methods*, 2009, **6**, 153–159.
3 R. Ando, H. Hama, M. Yamamoto-Hino, H. Mizuno and A. Miyawaki, *Proc. Natl. Acad. Sci. U. S. A.*, 2002, **99**, 12651–12656.
4 F. V. Subach, L. Zhang, T. W. Gadella, N. G. Gurskaya, K. A. Lukyanov and V. V. Verkhusha, *Chem. Biol.*, 2010, **17**, 745–755.
5 T. Grotjohann, I. Testa, M. Leutenegger, H. Bock, N. T. Urban, F. Lavoie-Cardinal, K. I. Willig, C. Eggeling, S. Jakobs and S. W. Hell, *Nature*, 2011, **478**, 204–208.
6 T. Brakemann, A. C. Stiel, G. Weber, M. Andresen, I. Testa, T. Grotjohann, M. Leutenegger, U. Plessmann, H. Urlaub, C. Eggeling, M. C. Wahl, S. W. Hell and S. Jakobs, *Nat. Biotechnol.*, 2011, **29**, 942–947.
7 V. Adam, M. Lelimousin, S. Boehme, G. Desfonds, K. Nienhaus, M. J. Field, J. Wiedenmann, S. McSweeney, G. U. Nienhaus and D. Bourgeois, *Proc. Natl. Acad. Sci. U. S. A.*, 2008, **105**, 18343–18348.
8 B. Wu, K. D. Piatkevich, T. Lionnet, R. H. Singer and V. V. Verkhusha, *Curr. Opin. Cell Biol.*, 2011, **23**, 310–317.
9 D. M. Shcherbakova, O. M. Subach and V. V. Verkhusha, *Angew. Chem., Int. Ed.*, 2012, **51**, 10724–10738.
10 T. J. Gould, S. T. Hess and J. Bewersdorf, *Annu. Rev. Biomed. Eng.*, 2012, **14**, 231–254.
11 C. Xu, W. Zipfel, J. B. Shear, R. M. Williams and W. W. Webb, *Proc. Natl. Acad. Sci. U. S. A.*, 1996, **93**, 10763–10768.
12 H. Tsutsui, S. Karasawa, H. Shimizu, N. Nukina and A. Miyawaki, *EMBO Rep.*, 2005, **6**, 233–238.
13 M. Schneider, S. Barozzi, I. Testa, M. Faretta and A. Diaspro, *Biophys. J.*, 2005, **89**, 1346–1352.
14 J. Folling, V. Belov, D. Riedel, A. Schonle, A. Egner, C. Eggeling, M. Bossi and S. W. Hell, *ChemPhysChem*, 2008, **9**, 321–326.
15 S. Ivanchenko, C. Rocker, F. Oswald, J. Wiedenmann and G. U. Nienhaus, *J. Biol. Phys.*, 2005, **31**, 249–259.
16 A. Vaziri, J. Tang, H. Shroff and C. V. Shank, *Proc. Natl. Acad. Sci. U. S. A.*, 2008, **105**, 20221–20226.
17 K. Isobe, H. Hashimoto, A. Suda, F. Kannari, H. Kawano, H. Mizuno, A. Miyawaki and K. Midorikawa, *Biomed. Opt. Express*, 2010, **1**, 687–693.
18 T. M. P. Hartwich and J. Bewersdorf, in preparation.
19 M. S. Gunewardene, F. V. Subach, T. J. Gould, G. P. Penoncello, M. V. Gudheti, V. V. Verkhusha and S. T. Hess, *Biophys. J.*, 2011, **101**, 1522–1528.
20 N. G. Gurskaya, V. V. Verkhusha, A. S. Shcheglov, D. B. Staroverov, T. V. Chepurnykh, A. F. Fradkov, S. Lukyanov and K. A. Lukyanov, *Nat. Biotechnol.*, 2006, **24**, 461–465.
21 S. A. McKinney, C. S. Murphy, K. L. Hazelwood, M. W. Davidson and L. L. Looger, *Nat. Methods*, 2009, **6**, 131–133.
22 F. V. Subach, V. N. Malashkevich, W. D. Zencheck, H. Xiao, G. S. Filonov, S. C. Almo and V. V. Verkhusha, *Proc. Natl. Acad. Sci. U. S. A.*, 2009, **106**, 21097–21102.

